ECS Transactions, 58 (2) 191-198 (2013)
10.1149/05802.0191ecst ©The Electrochemical Society

The Soft Chemical Route Improving IT-SOFC Cathode Performance: The Lanthanum Barium Cobaltite Case.

Diana Garcés and Liliana Mogni

Instituto Balseiro-CONICET- CNEA Centro Atómico Bariloche
CNEA, S. C. de Bariloche 8400,

In this work we studied the oxygen reduction mechanism in three cathodes: cubic $La_{0.5}Ba_{0.5}CoO_{3-\delta}$ obtained by Solid State Reaction (SSR) in air at 1100 ºC; a phase with cationic order, laminar structure and tetragonal symmetry, $LaBaCo_2O_{6-\delta}$, was obtained by SSR under inert gas at 1150ºC. An intermediate compound with the same nominal composition was obtained at lower temperature by a soft chemical route involving a sol-gel process. Despite that the crystal structures of the oxides obtained by SSR are different, their microstructures are similar but quite different to that obtained by the soft chemical route. The area specific resistance (ASR) as a function of pO_2 was studied at 700°C by Electrochemical Impedance Spectroscopy (EIS). We found that both, crystal structure and microstructure affect strongly the ASR. Whereas cubic perovskite showed lower ASR than tetragonal, the ASR of the oxide obtained by the chemical route decreased almost one order of magnitude at higher pO_2, respect to that obtained by conventional SSR.

Introduction

Different cobaltites with perovskite (ABO_3) related structures have been proposed as materials for high and intermediate temperatures electrochemical applications (1-4). The high ionic and electronic conductivity of these materials together with their good oxygen exchange properties make them suitable to substitute conventional oxygen electrodes working in Intermediate Temperature Solid Oxide Fuel Cell (IT-SOFC).

In this work we explore the 50%Ba-50%La substitution in A site of a Co-rich perovskite with nominal composition $La_{0.5}Ba_{0.5}CoO_{3-\delta}$. Recent works showed that, by controlling the synthesis parameter, it is possible to controll the crystal structure of this composition. Thus, whereas in air atmosphere at 1100 ºC a cationic disordered phase with cubic structure ($La_{0.5}Ba_{0.5}CoO_{3-\delta}$) was obtained, under inert gas Ar at 1150 ºC a cationic ordered phase with laminar structure and tetragonal symmetry was obtained ($LaBaCo_2O_{6-\delta}$) (5-7). These different structures arise from the difference between ionic radii of both cations (r_{La3+}=1.36 Å and r_{Ba2+} = 1.61 Å) and the unlike capability to accommodate oxygen vacancies of these compounds.

Recently, S. Pang et al. found that, while the electrical conductivity for cationic disordered $La_{0.5}Ba_{0.5}CoO_{3-\delta}$ phase is higher than that of ordered $LaBaCo_2O_{6-\delta}$, the ASR is

lower (8-10). For the latter, the ASR reaches values of 0.0086 Ωcm^{-2} for the ordered (9) and 0.013 Ωcm^{-2} for the disordered (10) at 800 °C in air.

In this work, we studied both, the $La_{0.5}Ba_{0.5}CoO_{3-\delta}$ and the $LaBaCo_2O_{6-\delta}$ obtained by conventional SSR and we also essayed a new chemical route involving a gel formation. This sol gel route allowed to reduce the synthesis temperature, to improve the microstructure and to reduce de Area Specific Resistance (ASR). The reason of this improvement was investigated in relation with the switch of oxygen reduction mechanism by studying the dependence of ASR with oxygen partial pressure.

Experimental

Synthesis and Characterization

We obtained three samples using two different methods: SSR and a sol-gel route named HMTA (11).

The SSR method used La_2O_3, $BaCO_3$, and Co_3O_4 as starting materials. These materials were milled at 500 rpm during 30 min using an Agatha container. The mixture underwent two different heat treatments:

- 1100 ºC for 12 h in air with a heating/cooling rate of 5°C/min, sample referred to as "LBC-1100 °C/Air".
- 1150 ºC for 24 h under Ar flow with a heating/cooling rate of 2°C/min, sample referred to as "LBC-1150 ºC/Ar".

The HMTA method is a chemical route involving a gel formation by polymerization of AcetylAetone (AcAc) and Hexametyltetramine (HMTA). This method started dissolving $BaCO_3$, La_2O_3 and $Co(CH_3COO)_2.4H_2O$ in acetic acid with AcAc and HMTA. Relation of organic ($C_o = C_{HMTA} + C_{acac}$) to inorganic ($C_i = C_{La+3} + C_{Ba+2} + C_{Co+2}$) materials was fixed at $C_o/C_i = 3.1$ Once a transparent solution was formed, it was heated at 80 °C until gel formation. This gel was burned at 450 °C during 2 h. Organic materials were calcinated at 750°C in air. The resulting powder was burned at 900°C under Ar flow during 24 h with a subsequent heat treatment in air at 400 °C to facilitate the oxygen incorporation. The resulting material was referred to as "LBC-900 ºC/Ar".

The crystal structures of final powders were analyzed by X-ray diffraction (XRD) using a Philips PW1700 diffractometer with Cu-Kα radiation. The microstructures were studied by Scanning Electron Microscopy (SEM) using a FEG-SEM FEI NanoSem microscope.

Electrochemical Characterization

The electrochemical response of all samples was evaluated by Electrochemical Impedance Spectroscopy (EIS) on symmetrical cells LBC/GDC/LBC (GDC, Gadolinium-Doped Cerium).

The symmetrical cells were prepared using dense GDC disc as electrolyte sintered at 1400 °C from commercial NexTech-Materials powders. The LBC electrode layers were deposited by spin coating. An intermediate layer of porous GDC was deposited between porous LBC and dense GDC in order to improve adherence between materials (12). While the GDC porous layers were calcined at 1400°C-1h, the cells were then annealied at 850°C during 1 h.

The EIS measurements were performed at 700 ºC changing oxygen partial pressure (pO_2) between 0.9 and 5 10^{-4} atm using an electrochemical device for pumping and sensing O_2. The EIS spectrums were collected using an Autolab-PGSTAT32 with a FRA2 module varying the frequency between 1 MHz y 0.1 mHz under a bias voltage of 0 V with 10 mV of amplitude.

Results and Discussion

Synthesis and Characterization

Figure 1 shows the XRD patterns of three samples. Pattern diffraction of LBC-1100 °C/Air sample could be indexed as cubic $La_{0.5}Ba_{0.5}CoO_{3-\delta}$ perovskite and the LBC-1150 ºC/Ar pattern as tetragonal $LaBaCo_2O_{6-\delta}$ layered perovskite. Bragg index of each peak was included in the graphic. On the contrary, the assignment of diffraction peaks was difficult to make for the LBC-900°C/Ar sample obtained by sol gel route due to the broadening of the peaks. Two different situations were considered: the coexistence of both, cubic and tetragonal phases or the formation of a single phase highly distorted. Structural refinements of diffraction peaks applying Rietveld method suggested that this compound belong to the tetragonal phase with a high strain responsible of peak broadening. This result should be confirmed by complementary diffraction techniques such as HR-TEM.

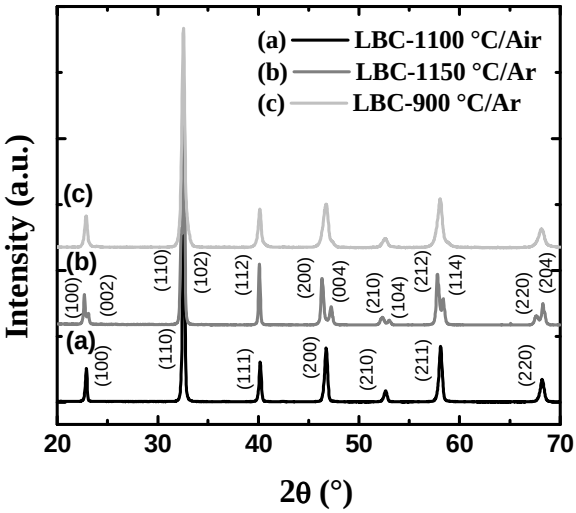

Figure 1. XRD of powders obtained by SSR: (a) LBC-1100 °C/Air and (b) LBC-1150 °C/Ar; and by HMTA sol gel route (c) LBC-900 °C/Ar.

Figure 2 shows SEM images of samples. Whereas, the microstructure of oxides obtained at 1100 ºC in air and at 1150 ºC in Ar look similar between them, they are quite different to that obtained by chemical route at 900 ºC in Ar. In both, LBC-1100 °C/Air and LBC-1150 °C/Ar samples, the SSR method yielded particles with size larger than 1 μm, while the chemical route allowed to reduce the particle sized under 200 nm.

Electrochemical Characterization

Figure 3 shows the impedance spectra of samples at 700 °C and different pO_2. As noticed, the polarization resistance of the sample obtained by chemical route decreased almost one order of magnitude at higher pO_2 respect to that obtained by SSR. As an example, considering the total ASR at 700 °C and in air (pO_2 = 0.21 atm), the values decreased down to 0.27, 0.11 and 0.04 Ωcm^{-2} for LBC-1150 °C/Ar, LBC-1100 °C/Air and LBC-900 °C/Ar, respectively.

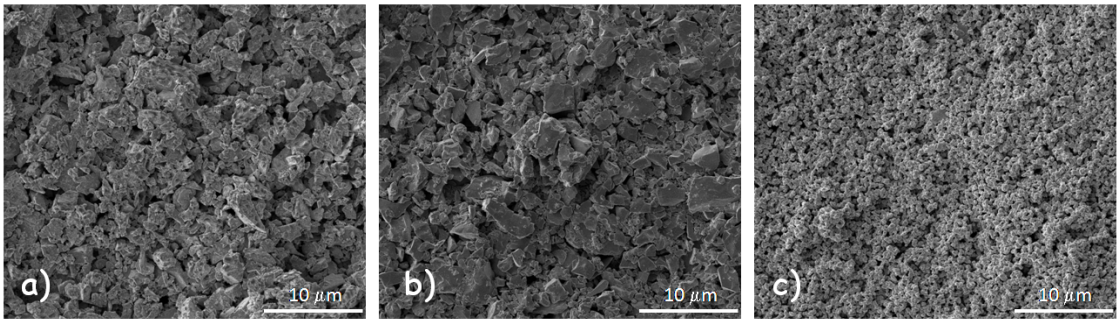

Figure 2. SEM images of powders obtained by SSR: (a) LBC-1100 °C/Air and (b) LBC-1150 °C/Ar; and by HMTA sol gel route (c) LBC-900 °C/Ar.

TABLE I. Electrical equivalent circuit applied to fit EIS spectrum at each pO_2 range.

Sample	pO_2 (atm)				
	$5\ 10^{-4}$	**0.12**	**0.21**	**0.37**	**0.87**
LBC-1100 °C/ Air	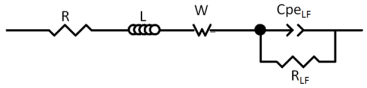 n_W = -0.35, n_{RCpe} = -0.93		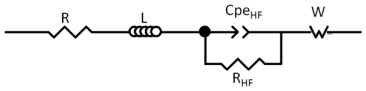 n_W = -0.35, n_{RCpe} = -0.04		
LBC-1150 °C/ Ar	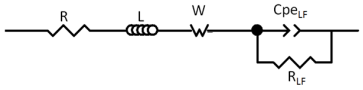 n_W = -0.42, n_{RCpe} = -0.37				
LBC-900 °C/Ar	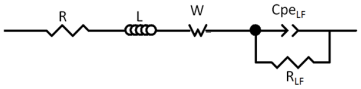 n_W = -0.23, n_{RCpe} = -1.06		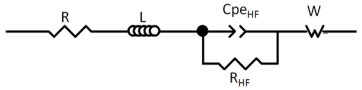 n_W = -0.23, n_{RCpe} = 0.09		

In all three samples, at least two contributions could be distinguished. The EIS spectra were fitted using electrical equivalent circuits. The equivalent circuits considered the electrolyte resistance (R), the inductance of connectors (L) and three electrodes contribution: a resistance (RHF) in parallel with a capacitive (CpeHF) to fit the high frequency arc (HF), a Warburg element at medium frequency and a second RCpe to fit the low frequency (LF) arc. The elements of electrical equivalent circuits used were

different depending on pO_2 values and sample. Each element varied with pO_2 in a different way according to process controlling the mechanism of reaction in each sample and frequency range. The variation of a process resistance with pO_2 followed a relationship as $R \propto pO_2^n$ (n ranging between -1 and 0) which could be assigned to O2 gas diffusion, O2 dissociative adsorption, O exchange at the electrode surface, O ion diffusion inside electrode or O ion transfer trough electrode/electrolyte interphase (13). The electrical equivalent circuits used in each case are listed in Table I.

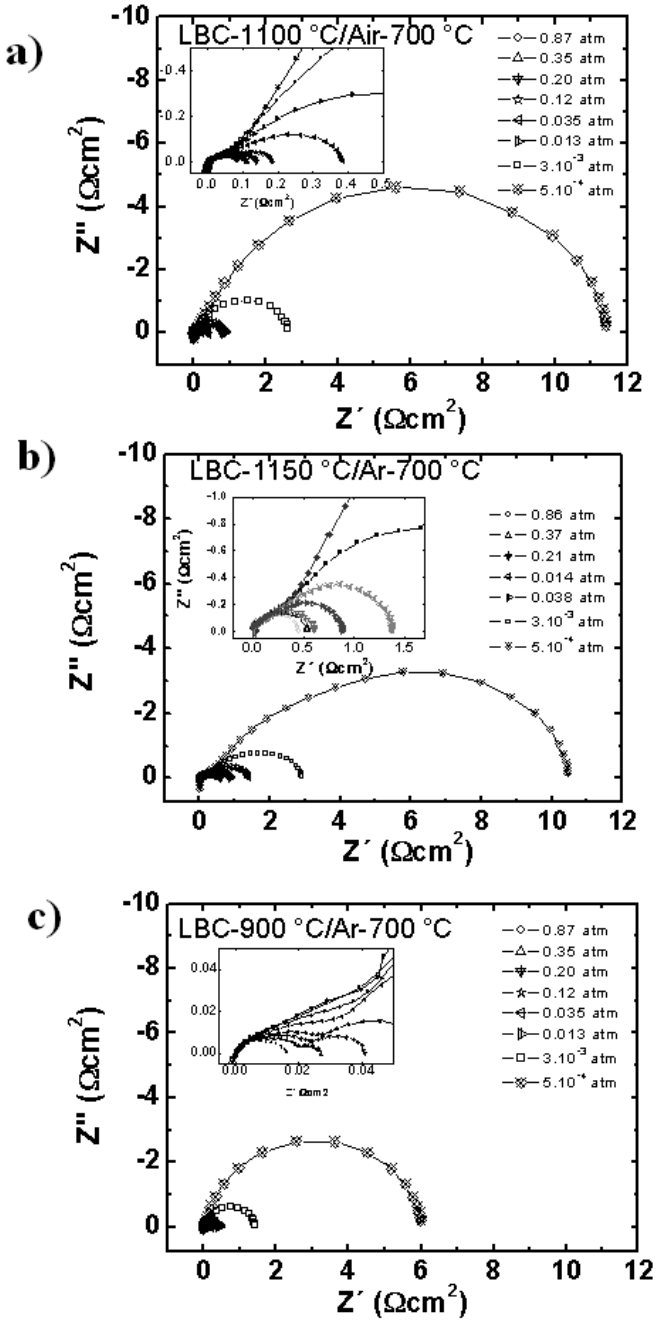

Figure 3. EIS spectra at 700 ºC as a function of pO_2 for samples obtained by SSR: (a) LBC-1100 °C/Air and (b) LBC-1150 °C/Ar; and by HMTA sol gel route (c) LBC-900 °C/Ar.

.

Figure 4 shows the log-log graphic of polarization resistance corresponding to each electrode contribution to the electrical equivalent circuit as a function of pO_2. The dependence of polarization resistance with pO_2 and the activation energy allowed proposing the nature of the different processes:

The high frequency contributions is a RCpe circuit only observed at high pO_2 for the LBC-1100 ºC/Air and LBC-900 ºC/Ar samples. The ASR values for this contribution did not show any dependence with pO_2 and this suggested that this contribution should be due to the charge transfer across the electrode/electrolyte interface. The lower value of ASR for LBC-900°C/Ar respect to that of LBC-1100°C/Air would be related to the fact that the lower sizes of LBC-900°C/Ar particles increases the contact area between both phases reducing the resistance associated to this process. We suppose that this process was not observed in LBC-1150°C/Ar because it is masked by the high resistance values of other contributions.

The intermediate frequency is a finite Warburg element. Usually, this kind of element is related to diffusive processes of ionic species inside the electrode material. However, in this case, due to the markedly dependence with pO_2, we suppose that it should be associated to oxygen bulk diffusion with some grade of co-limitation by oxygen surface exchange, depending on the sample microstructure. While comparing the values of Warburg resistance for LBC-1100 ºC/Air and LBC-1150 ºC/Ar and taking into account that these samples have similar microstructures, it seems to be clear that the crystal structure play a fundamental role in the oxygen diffusion process.

The low frequency process changed depending on sample microstructure and structure. For LBC-1100 ºC/Air and LBC-900 ºC/Ar samples the low frequency resistances depend as pO_2^{-1}, this behavior could be assigned to oxygen gas diffusion. In contrast, for LBC-1150ºC/Ar sample this resistance depends with ~ $pO_2^{-0.5}$, suggesting that the perfectly layered La/Ba distribution might induce a surface dissociative adsorption process limiting the electrode mechanism for this sample.

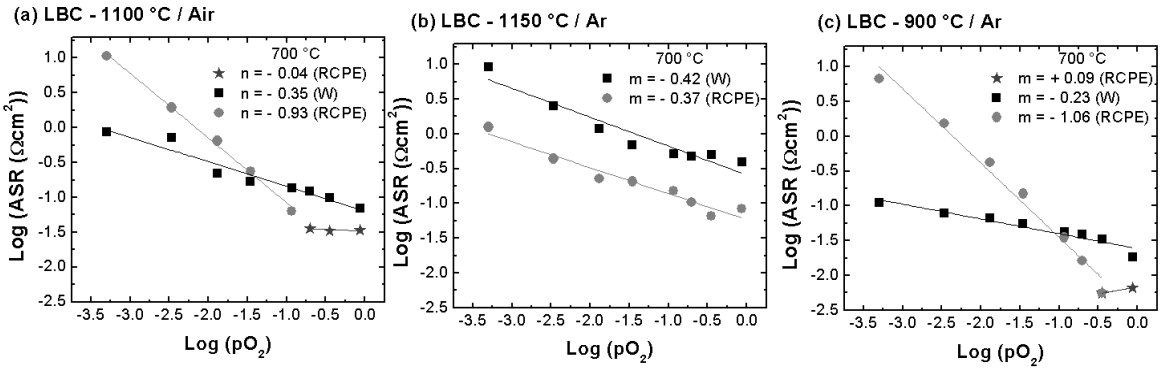

Figure 4. log(ASR) vs log(pO2) at 700 ºC for samples obtained by SSR: (a) LBC-1100 °C/Air and (b) LBC-1150 °C/Ar; and by HMTA sol gel route (c) LBC-900 °C/Ar.

The results discussed in this work clearly indicate a strong effect of crystal structure and microstructure in cathode resistances. However, these results are preliminary. Next works should include advanced method such as 3D FIB-SEM reconstruction to obtain detailed microstructure parameters and HR-TEM to obtain additional crystal structure

information. This way, trying to correlate the information obtained from these techniques with an electrochemical model representing the electrode response, we would be able to obtain more useful information about mechanism working and how to reduce cathode overpotentials (14).

Conclusion

The possibility of obtaining oxides with nominal composition 0.5La-0.5Ba-Co and different structures and microstructures, allowed to us to study the effect of both on the oxygen reduction mechanism of IT-SOFC cathode.

On one hand, while comparing two samples with similar microstructure but different crystal structure (LBC-1100 °C/Air and LBC-1150 °C/Ar) we could observed how the layered perovskite increases the polarization resistance associated with processes such as the oxygen ion diffusion and the dissociative adsorption. On the other hand, when a soft chemical route was used to obtain the oxides with lower particle size, the polarization resistance was reduced in almost one order of magnitude. In this case, the major contributions to polarization resistance were the oxygen ion diffusion inside the oxides at high pO_2 and the O_2 diffusion in gas phase at low pO_2.

Acknowledgments

This work was supported by CNEA (Argentine Atomic Energy Commission), CONICET (Argentine Research Council), National University of Cuyo and ANPCyT. The authors thank to the integrants of Division Caracterizacion de Materiales (Centro Atomico Bariloche) for their support and helpful discussion.

References

1. W. Zhou, R. Ran, and Z. Shao, *J. Power Sources* **192 (2)**, 231 (2009).
2. C. Setevich, L. Mogni, A. Caneiro, and F. Prado, *J. Electrochem. Soc.* **159 (1)**, B73 (2012).
3. A.Tarancón, S. Skinner, R. Chater, F. Hernández-Ramírez, and J. Kilner, *J. Mater. Chem.* **17**, 3175 (2007).
4. J.-H. Kim, L. Mogni, F. Prado, A. Caneiro, J. A. Alonso, and A. Manthiram, *J. Electrochem. Soc.***156 (12)**, B1376 (2009).
5. T.Nakajima, M. Ichihara, and Y. Ueda, *J. Phys. Soc. Jpn.* **74 (5)**, 1572 (2005).
6. E. Rautama, V. Caignaert, Ph. Boullay, A. Kundu, V. Pralong, M. Karppinen, C. Ritter, and B. Raveau, *Chem. Mater.* **21**, 102 (2009).
7. E. Rautama, Ph. Boullay, A. Kundu, V. Caignaert, V. Pralog, M. Karppinen, and B. Raveau, *Chem. Mat.* **20**, 2742(2008).
8. S.L. Pang, X. N. Li, Q. Wang, and Q.Y. Zhang, *Mater. Chem. Phys.* **131**, 642 (2012).
9. S.L. Pang, X. Jiang, X. Li, Z. Su, H. Xu, Q. Xu, and C. Chen, *Int. J. Hydrogen Energy* **37**, 6836 (2012).

10. S. L. Pang, X. Jiang, X. Li, Q. Wang, and Z. Su, *Int. J. Hydrogen Energy* **37**, 2157 (2012).
11. L. Baqué, A. Caneiro, M.S. Moreno, and A. Serquis, *Electrochem. Comm.* **10** 1905 (2008).
12. C. Setevivh, L. Mogni, A. Caneiro, and F. Prado, *Int. J. Hydrogen Energy;* **37** 14895 (2012).
13. S. B. Adler, *Chemical Reviews*. 104 (2004) 4791–843.
14. C. R. Kreller, M.E. Drake, S. B. Adler, H.-Y. Chen, H.-C. Yu, K. Thornton, J. R. Wilson and S. A. Barnett, *ECS Transactions*, 35 (1) 815-822 (2011).